JGR Atmospheres

RESEARCH ARTICLE
10.1029/2024JD041233

The Relative Role of Indian and Pacific Tropical Heating as Seasonal Predictability Drivers for the North Atlantic Oscillation

Retish Senan[1], Magdalena A. Balmaseda[1], Franco Molteni[1], Timothy N. Stockdale[1], Antje Weisheimer[1,2], Stephanie Johnson[1], and Christopher D. Roberts[1]

[1]European Centre for Medium-Range Weather Forecasts, Reading, UK, [2]National Centre for Atmospheric Science (NCAS), Atmospheric, Oceanic and Planetary Physics (AOPP), University of Oxford, Oxford, UK

Key Points:

- Large ensemble seasonal forecasts reveal a predictable link between tropical heating and the NAO via a flow-dependent stratospheric pathway
- The impact of Indian Ocean heating on the NAO can be stronger than that of El Niño in the presence of an anomalously strong stratospheric pathway
- Competition between basins, flow-dependent response, and intrinsic variability contribute to the uncertainty in seasonal forecasts of NAO

Supporting Information:

Supporting Information may be found in the online version of this article.

Correspondence to:

R. Senan,
retish.senan@ecmwf.int

Citation:

Senan, R., Balmaseda, M. A., Molteni, F., Stockdale, T. N., Weisheimer, A., Johnson, S., & Roberts, C. D. (2024). The relative role of Indian and Pacific tropical heating as seasonal predictability drivers for the North Atlantic Oscillation. *Journal of Geophysical Research: Atmospheres*, *129*, e2024JD041233. https://doi.org/10.1029/2024JD041233

Received 25 MAR 2024
Accepted 7 SEP 2024

Abstract Understanding the predictability drivers for the North Atlantic Oscillation (NAO) during boreal winter at seasonal time scales remains challenging. This study uses large ensembles with the ECMWF seasonal forecasting system to investigate the relative impact of tropical Indian and Pacific heating on NAO predictability by examining the tropical forcing, teleconnection pathways, and sources of uncertainty. We select three case studies - 1997/98, 2015/16 and 2019/20 - with strong Indian Ocean heating anomalies, but with different El Niño conditions. We show that in 2019/20, with neutral ENSO conditions, Indian Ocean SSTs favor a positive NAO response via stratospheric and tropospheric pathways. In the cases with strong El Niño, we find contrasting results: in 1997/98, the Pacific forcing dominates, producing a negative NAO. In 2015/16, despite the strong El Niño, the Indian Ocean forcing dominates, leading to a positive NAO via intensification of the stratospheric polar vortex (SPV). While the stratospheric pathway exhibits varying responses to Indian Ocean forcing - being weaker in 1997/98 and strongest in 2015/16, the Indian Ocean-related tropospheric pathway remains robust along the Pacific subtropical jet across years. However, there is destructive interference between teleconnections from Indian and Pacific SST anomalies in both the tropospheric and stratospheric pathways. The competing effects of tropical heating in both basins, uncertainties in the Rossby wave response to tropical heating and SPV variability contribute to uncertainty in seasonal NAO predictions. The flow-dependent nature of the stratospheric pathway underscores the complexity of seasonal forecast predictability, and the existence of windows of opportunity.

Plain Language Summary The NAO is a phenomenon that manifests as a pressure see-saw in the North Atlantic, affecting the seasonal climate in many parts of the northern hemisphere. In this study, we demonstrate that the predictability of the phases of the NAO can be affected by the remote and opposing influence of surface temperatures in the tropical Indian and Pacific oceans, which propagate via the troposphere and stratosphere. This interplay, in turn, contributes to the uncertainty of seasonal forecasts of the NAO.

1. Introduction

The boreal winter of 2019/20 was notable for the accuracy of many operational seasonal forecasting systems, including the European Centre for Medium-Range Weather Forecasts (ECMWF) seasonal forecasting system (SEAS5, Johnson et al., 2019), which consistently predicted the positive phase of the NAO, particularly for the late winter period (Lee et al., 2020). The situation stood out in several aspects: (a) a robust forecast signal over Europe; (b) model consensus over this region; and (c) the accuracy of the forecast signal over this often low-skill region. Why were the seasonal forecasts successful on this occasion? What were the predictable drivers at work?

There was no significant El Niño Southern Oscillation (ENSO) in 2019/20, but anomalously warm conditions occurred over the Indian Ocean - a result of an exceptionally strong positive Indian Ocean Dipole (IOD) event during boreal autumn (Wang et al., 2020), whose positive sea surface temperature (SST) anomaly in the western central Indian Ocean persisted into the winter. These SST conditions were well captured by SEAS5.

Past studies have demonstrated the important role of the Asian mid-latitude jet waveguide in mediating tropical-extratropical teleconnections affecting the positive phase of NAO via eastward propagating Rossby waves (Bader & Latif, 2005; Fletcher & Cassou, 2015, FC15 in what follows). Such a mechanism is one of the pathways identified in the study of Hardiman et al. (2020) who show that the strong positive IOD event of October-November 2019 was a key driver of the positive NAO response in Winter 2019/20. Using climate simulations,

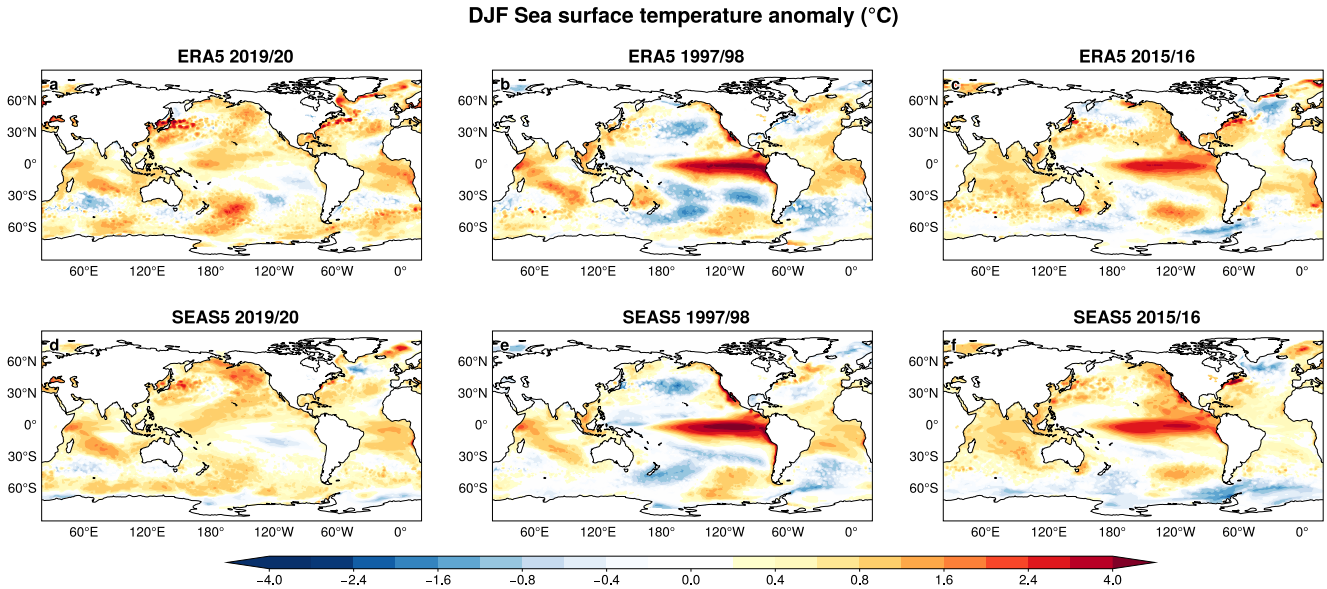

Figure 1. December to February (DJF) seasonal mean sea surface temperature anomaly (°C) from ERA5 (a–c) and ensemble mean of SEAS5 (d–f) for 2019/20 (left column), 1997/98 (middle column) and 2015/16 (right column).

FC15 identified a stratospheric pathway linking the heating in the Indian Ocean with the NAO, via its influence on the SPV. This mechanism also operates at subseasonal timescales (e.g., Domeisen et al., 2020; Garfinkel et al., 2014; Roberts et al., 2023). Further, as documented in many studies (e.g., FC15; Fletcher & Kushner, 2011; Molteni et al., 2015), anomalous heating in the Indian Ocean during middle-to-late winter is associated with a positive NAO response in contrast to the canonical negative NAO response to El Niño in the Tropical Pacific (Brönnimann, 2007; Toniazzo & Scaife, 2006). It is therefore unclear what influence the Indian Ocean heating would have on the NAO in the presence of El Niño.

In this study, we compare the boreal winter 2019/20 response with that in 1997/98 and 2015/16, when there were also strong warm SST anomalies in the Indian Ocean, but with extreme El Niño conditions in the Pacific (Figures 1a–1c). In all three cases, the coupled seasonal forecasts reproduced well the intensity and structure of the SST anomalies (Figures 1d–1f). To elucidate the role of tropical SST forcing from the Indian and Pacific basins on winter-time NAO seasonal mean anomalies, we perform a suite of seasonal retrospective forecast experiments forced by suppressing the SST anomalies in different tropical basins. To facilitate different combinations of SST forcing, these experiments are performed in uncoupled mode, although we acknowledge that the lack of coupled feedback in both tropics and extratropics can affect the properties of the diabatic heating.

Both the experimental framework and the research questions addressed in this study are different from those of FC15 and Hardiman et al. (2020). Unlike FC15, which deduces impact based on long climate simulations, this paper focuses on specific cases and seasonal time scales. While Hardiman et al. (2020) also focuses on seasonal time scales, their emphasis was on the specific case of 2019/20 using a coupled model, whereas our approach involves uncoupled experiments for three different winters to compare the relative influence of the Pacific and Indian Ocean SST in different conditions. Notably, our study uses dedicated experiments to specifically investigate the interference of signals from the Pacific and the Indian Oceans and the flow-dependent nature of the response to Indian Ocean SST anomalies (e.g., whether the response to the Indian Ocean is robust or modulated by other factors, such as the presence of El Niño). In addition, this study also includes an analysis of the sources of uncertainty in the NAO forecasts.

The paper is structured as follows: Section 2 introduces the experimental setup and methodology. In Section 3, we discuss the results, that includes the characterization of the atmospheric circulation in the three selected years, the isolation of the influences of the SST in the Indian Ocean and Tropical Pacific and their respective teleconnection pathways (Section 3.1), the flow dependency of that response (Section 3.2) and analysis of intrinsic atmospheric variability in the forecast ensembles (Section 3.3). The paper concludes with a summary of the findings in Section 4.

Table 1
List of Reference/Attribution Experiments

Regional anomaly year/ Climatology (CLIM)		Background conditions (BC) year		
		2019/20	1997/98	2015/16
INDIAN	2019/20	R20	I20_BC98	I20_BC16
	1997/98	I98_BC20	R98	–
	2015/16	I16_BC20	–	R16
	CLIM	IC20	IC98	IC16
PACIFIC	CLIM	PC20	PC98	PC16

2. Experiments and Methodology

We use the atmosphere-only version of SEAS5, ECMWF's fifth generation seasonal forecast system, with the same configuration as used in SEAS5 reforecasts (see Johnson et al., 2019 for more details). The reference experiments (Table 1), abbreviated as R20 (ECMWF, 2023i), R98 (ECMWF, 2023g) and R16 (ECMWF, 2023h), are forced by daily SST from the ECMWF ERA5 reanalysis (Hersbach et al., 2020) during November to February of 2019/20, 1997/98 and 2015/16 respectively.

To isolate the impact of tropical heating we perform attribution experiments that involve replacing the daily SST over a given tropical basin (Indian or Pacific, 30°S–20°N) with a daily climatology, estimated as average of daily ERA5 SST values over the period 1981–2016. These experiments are abbreviated as IC20 (ECMWF, 2023c), IC98 (ECMWF, 2023a) and IC16 (ECMWF, 2023b) when forced by daily climatological SST over the tropical Indian Ocean. Similarly, PC20 (ECMWF, 2023f), PC98 (ECMWF, 2023d) and PC16 (ECMWF, 2023e) refer to experiments forced by daily climatological SST over the tropical Pacific Ocean. We also conducted equivalent experiments by removing the SST anomaly over the tropical Atlantic in 2019/20, but the impact was small, and the results are not reported here.

We conduct another set of complementary experiments specifically to address the flow-dependent impact of the SST anomaly over a given basin. Thus, experiments I20_BC98 (ECMWF, 2024a) and I20_BC16 (ECMWF, 2024b) are designed to quantify the impact of the 2019/20 Indian Ocean SST anomaly with the background conditions (BCs) of 1997/98 and 2015/16 respectively. Conversely, experiments I98_BC20 (ECMWF, 2024c) and I16_BC20 (ECMWF, 2024d) have the 1997/98 and 2015/16 Indian Ocean SST anomalies with the BCs of 2019/20. In these experiments, the BCs include SST and sea-ice anomalies in basins other than the Indian Ocean, as well as land and atmospheric initial conditions and radiative forcing. Therefore, the BCs in these experiments are time varying and should not be confused with a background climatological mean state.

All experiments are initialized on 01-November with a large ensemble size of 101 members. This large ensemble size was necessary due to the low signal-to-noise ratio in the seasonal predictions of NAO and SPV, as illustrated in Figure S1 in Supporting Information S1, consistent with Eade et al. (2014).

To determine the impact of SST anomalies from the different basins, we compute the ensemble mean differences between the reference (R) and attribution (IC/PC) experiments. We use December to February (DJF) mean 500 hPa Geopotential height (Z500) anomaly and the NAO index to diagnose impact. The NAO index is calculated as the projection of model DJF Z500 anomaly onto the first EOF of ERA5 Z500 over the North Atlantic domain (90°W–40°E, 20°N–80°N) normalized by its standard deviation. This definition follows Hurrell et al. (2003) and is the same as used for the ECMWF operational seasonal forecast products (Stockdale, 2021) but updated to use ERA5. Comparison with two different mean sea level pressure-based definitions of the NAO index (Dunstone et al., 2016; Li & Wang, 2003) indicate consistency with the Z500-based index (Figure S2 in Supporting Information S1). To gain insight into processes affecting the NAO signal and its uncertainty, we use intra-ensemble diagnostics, wherein composite differences between the members with highest and lowest values of the NAO index are analyzed. To evaluate the tropospheric teleconnection pathway, we utilize the DJF mean 200 hPa meridional velocity anomaly. To illustrate the stratospheric pathway and impact on the SPV, we examine a vertical section of the DJF mean zonal mean zonal wind anomaly at 60°N. Intra-ensemble diagnostics and comparison between different years are used to elucidate the relationship between the Indian Ocean and the NAO signal and uncertainty components. Anomalies are based on a 1981–2016 climatology.

3. Impact of Tropical Heating Anomalies on the NAO

To validate the experimental methodology, we first verify whether the model can reproduce the observed anomalies across the three cases considered. The observed neutral ENSO conditions in the tropical Pacific in 2019/20, El Niño conditions in 1997/98 and 2015/16, and warm anomalies in the tropical Atlantic and Indian Oceans were accurately forecast by SEAS5 (Figures 1d–1f). The SST-induced precipitation anomalies are largely consistent with ERA5, although some differences are evident (Figure 2). The wet anomalies in the west central Indian Ocean in 2019/20, the east-west dipole like-anomalies in the equatorial Indian Ocean in 1997/98, the

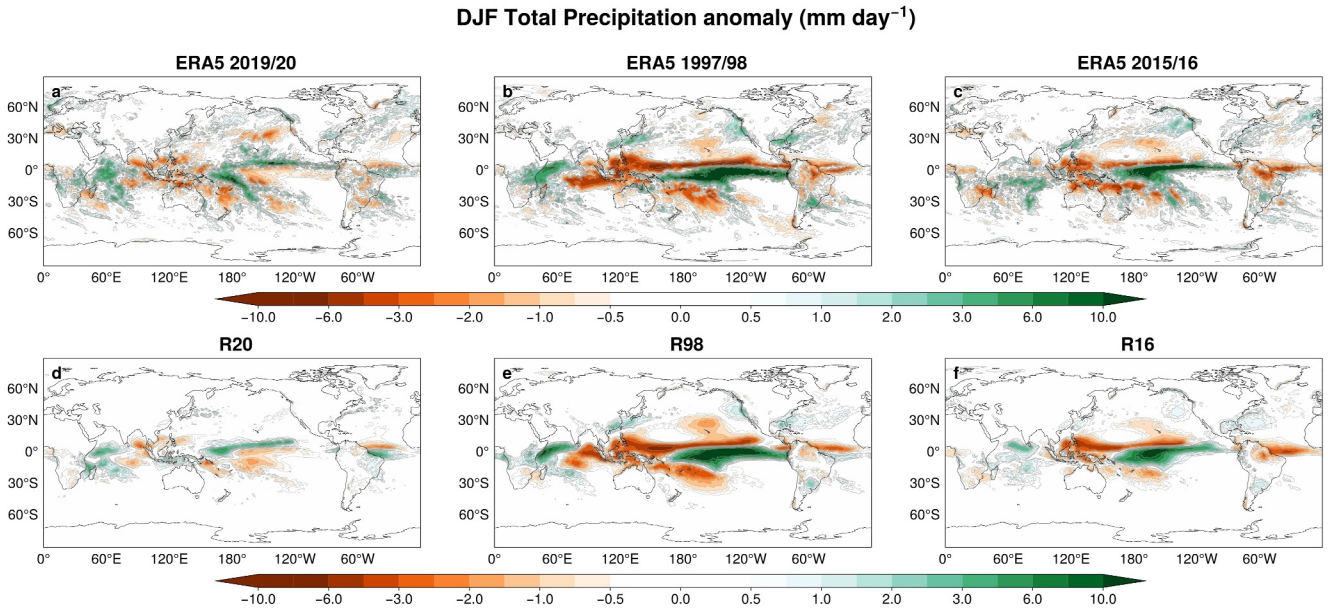

Figure 2. DJF seasonal mean total precipitation anomaly (mm day^{-1}) in (a–c) ERA5 and (d)–(f) ensemble mean of the reference experiments (R) for 2019/20 (left column), 1997/98 (middle column) and 2015/16 (right column).

ENSO related anomalies in the Pacific in 1997/98 and 2015/16, and the anomalies in the equatorial Atlantic in all 3 years are well-captured. However, differences in precipitation in critical deep convection regions such as the Maritime Continent may affect the model teleconnections. Figure 3 shows the DJF mean Z500 anomalies in ERA5 and the reference experiments in the three winters. The upper-air circulation anomalies in ERA5 associated with a positive NAO in 2019/20 (Figures 3a) and 2015/16 (Figure 3c), as well as a weakly negative NAO in 1997/98 (Figure 3b), are reasonably well reproduced by the ensemble mean of the reference experiments (R20, R98 and R16 in Figures 3d–3f), although the amplitude of the ensemble mean is weaker than in ERA5. The lower amplitude in the NAO pattern in R20 may be due to the displacement of the negative Z500 anomaly, which in R20 is centered to the west of the British Isles. Additionally, the anomalies at high latitudes in R20 do not correspond as well to those in ERA5. Nevertheless, over the North Atlantic-European sector (90°W–40°E, 20°N–90°N), the

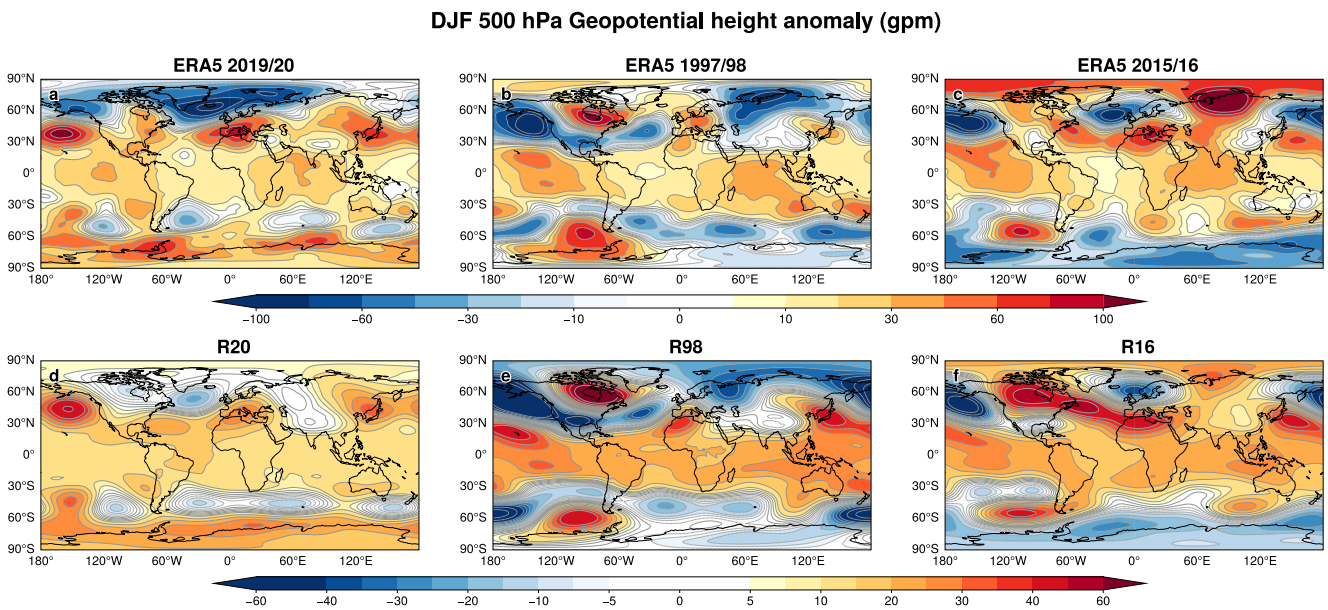

Figure 3. Same as Figure 2, but for Geopotential height anomaly (gpm).

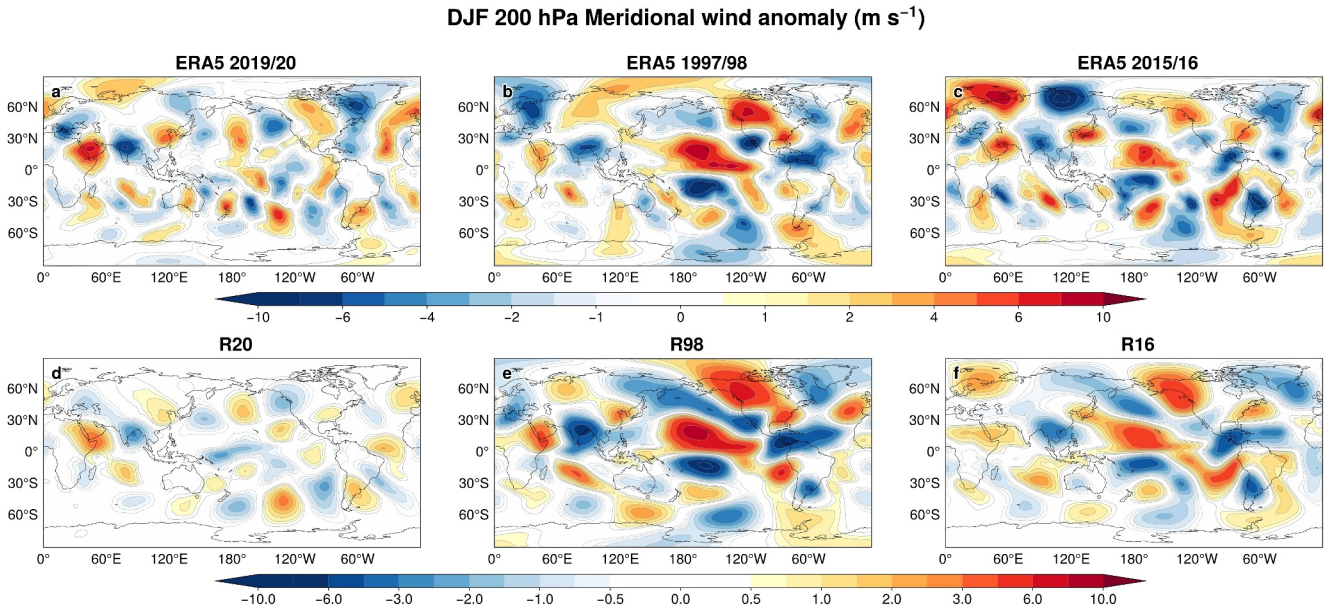

Figure 4. Same as Figure 2, but for 200 hPa meridional wind anomaly (m s^{-1}).

reference experiments have spatial correlations of 0.72, 0.77 and 0.62, respectively, against ERA5 (see also Figure S3 in Supporting Information S1). The fidelity of the NAO index in the model is further discussed in Section 3.1.

To verify the representation of tropospheric pathways associated with tropical heating via eastward propagating Rossby wave trains (e.g., Abid et al., 2021), we compare the 200 hPa meridional velocity in ERA5 and the reference experiments (Figure 4). Both ERA5 and reference experiments show the presence of a tropospheric pathway in 2019/20 (Figures 4a and 4d) consistent with Hardiman et al. (2020). The Rossby wave train is very different in the ENSO years (both in observations and experiments), with larger amplitude over the Northeastern Pacific (Figures 4b, 4c, 4e and 4f) in the form of a north-eastward long Rossby wave train that is usually associated with the canonical response to ENSO-related tropical Pacific SST anomalies (Trenberth et al., 1998). It is reassuring that the model can capture the observed anomaly and the differences among the 3 years considered, indicating that in these cases, errors in the atmospheric mean state did not contaminate the forecast of the anomalies. We also note that although SEAS5 exhibits biases in the position of the summer jet, these biases are relatively small during DJF (Johnson et al., 2019), at least on the seasonal time scales (Vitart et al., 2022).

3.1. Relative Impact of the Indian and Pacific SST Anomalies

We now analyze the differences between the reference experiments and the regional SST attribution experiments to gain insight into the impact of tropical SST anomalies from the Indian and Pacific Oceans on DJF seasonal atmospheric anomalies. Here we discuss the impact on Z500 (Figure 5), the SPV and NAO index (Figure 6), and 200 hPa meridional wind (Figure 7).

The impact of an anomalously warm tropical Indian Ocean in 2019/20 is to strengthen the wintertime positive NAO, as shown by the difference between the R20 and IC20 experiments (Figures 5a and 6g). The positive NAO and SPV are strengthened by the presence of the Indian Ocean forcing (Figure 6a) and weakened by the forcing from the Pacific Ocean (Figure 6d). This is consistent with the findings of FC15 in climate simulations, where the tropical heating over the Indian Ocean during DJF 2019/20 induces a strengthening of the SPV favoring positive NAO conditions. In 1997/98, the Indian Ocean favored positive NAO conditions as well (Figure 5b), but its influence was overcome by the canonical negative NAO response associated with El Niño heating in the Pacific (Domeisen et al., 2019) (Figure 5e) which also favors strengthening of the SPV (Figure 6e), consistent with Butler et al. (2014). In contrast, in 2015/16, there is a very strong stratospheric impact resulting from the Indian Ocean forcing (Figure 6c) which leads to a positive NAO (Figures 5c and 6i), thus dominating over the impact of the strong El Niño in the Pacific, which would have favored a negative NAO. Destructive interference between

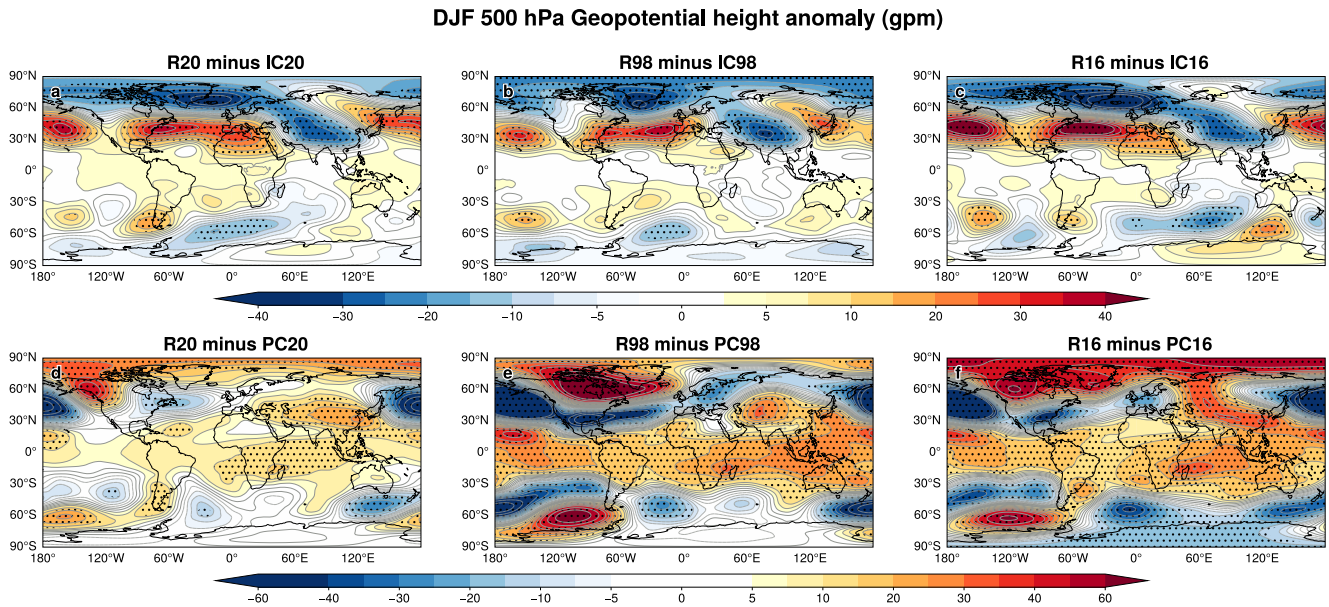

Figure 5. DJF seasonal mean 500 hPa Geopotential height anomaly (gpm) plotted as difference between ensemble means of the (a)–(c) R and Indian Ocean SST attribution (IC) experiments and (d)–(f) R and Pacific SST attribution (PC) experiments, for 2019/20 (left column), 1997/98 (middle column) and 2015/16 (right column). Stippled areas are significant at 1% based on a two-tailed Student's *t*-test.

opposing signals might be expected to increase the spread in the NAO. If this were the only source of NAO uncertainty, one would expect a smaller NAO spread for single-forcing experiments with a large impact on the NAO. This is indeed the case for the single forcing experiments IC98 and PC16 (Figures 6h and 6i). However, this does not apply to IC20/PC20 that have similar spread as R20, nor to IC16 which has comparable spread to R16. This suggests that destructive interference between basins is not the only source of uncertainty in the NAO.

The impact of the Indian and tropical Pacific Ocean SST anomalies on the tropospheric pathway in the three years is illustrated by the differences in 200 hPa meridional wind (Figure 7). The Indian Ocean SST anomalies favor a systematic strengthening of the Rossby wave train compared to the reference experiments (top panels in Figure 7), with a localized negative anomaly over the northeast Pacific, south of Alaska (see boxes in Figure 7 for guidance). As expected, the Rossby wave train triggered by the tropical Pacific anomaly has a larger amplitude in the ENSO years (bottom panels of Figure 7) but is in phase opposition with that arising from the Indian Ocean in all 3 years (Figures 7d–7f). Therefore, in the 3 years, there is destructive interference in the tropospheric teleconnection pathway between the tropical Indian and Pacific Oceans, such that during the two ENSO years, the Pacific forcing dominates the tropospheric pathway, but not so in 2019/20.

In summary, there are destructive interferences between the teleconnections from the Indian and Pacific SST anomalies in the 3 years, both in the tropospheric and stratospheric pathways. The Indian Ocean-related tropospheric pathway appears quite robust across years, particularly along the Pacific subtropical jet, with pattern and amplitude that does not depend on the background conditions, albeit with some discernible differences over the North Atlantic. In contrast, the stratospheric pathway shows substantial variability in the response to the Indian Ocean SST anomalies from year to year, being weakest in 1997/98 and strongest in 2015/16. This flow-dependent nature of the SPV response adds a new perspective to the canonical response described in FC15. While a thorough investigation of the reasons for this flow dependence is beyond the scope of this study, the following section attempts to separate the possible impact of the characteristics of the Indian Ocean SST anomalies in the different years from the dependence of the response to other background conditions.

3.2. Impact of Indian Ocean SST Anomaly Versus Background Conditions

While Indian Ocean heating contributes to the strengthening of the SPV in the 3 years (Figures 6a–6c), the impact is weaker in 1997/98 and stronger in 2015/16, compared to 2019/20. We investigate two possibilities for this behavior: (a) the impact of the time varying background conditions (BCs) in the 3 years and (b) the impact of the

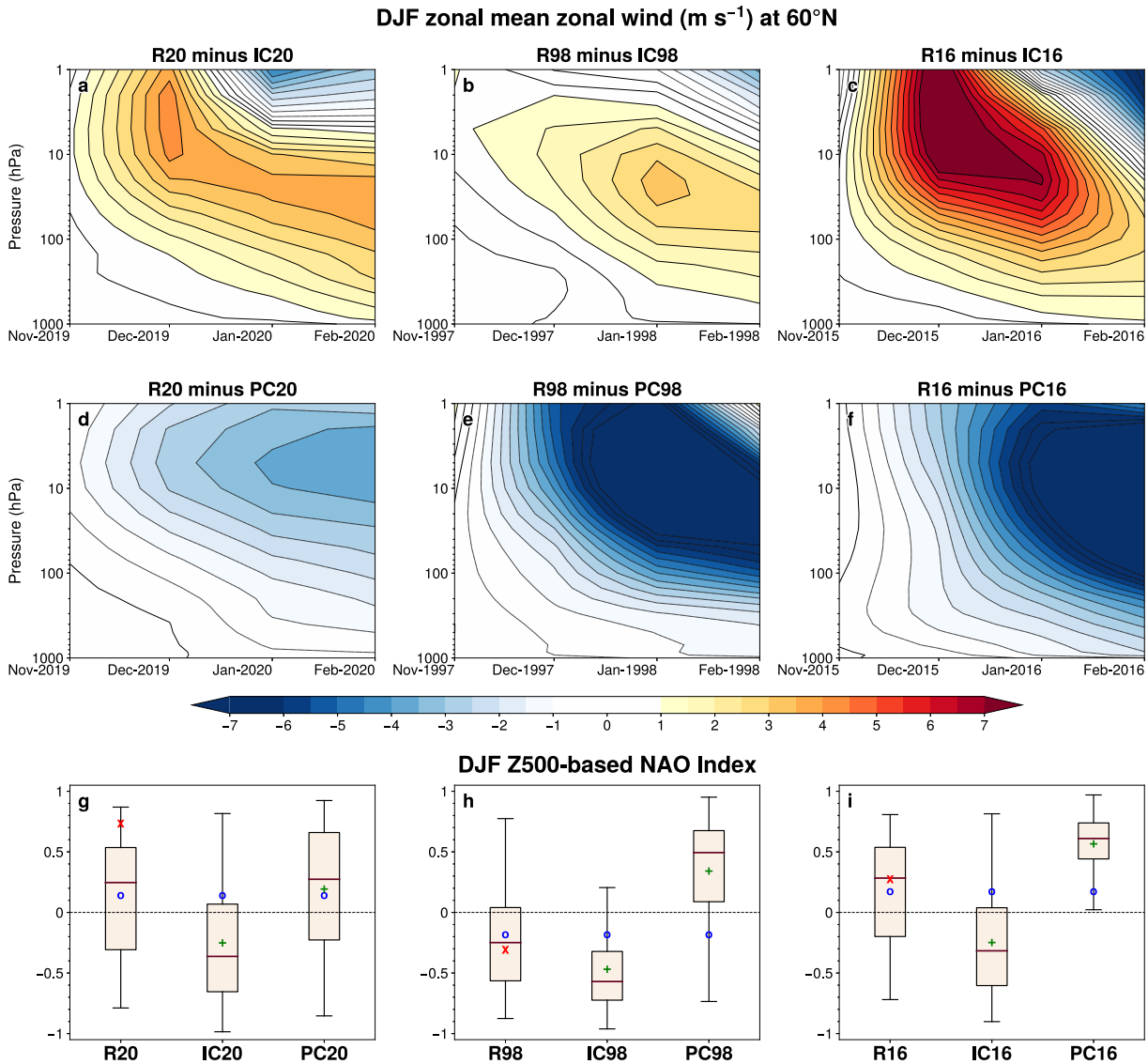

Figure 6. DJF seasonal mean zonal mean zonal wind (m s^{-1}) at 60°N plotted as the difference between ensemble means of the R and IC/PC experiments for (a)–(d) 2019/20, (b)–(e) 1997/98 and (c)–(f) 2015/2016. Also plotted in (g)–(i) are the box-and-whisker plots of the DJF mean NAO index for the R, IC, and PC experiments. NAO indices from ERA5 (Red cross) and the ensemble means from the R (Blue circles) and the IC/PC (Green plus signs) experiments are overlaid.

Indian Ocean heating anomalies in the 3 years. As explained in Section 2, background conditions include SST and sea-ice anomalies in basins other than the Indian Ocean, land and atmospheric initial conditions and radiative forcing.

Figure 8 is designed as an "impact matrix" with panels in the top row showing the impact of the BCs by comparing sensitivity experiments with the same Indian Ocean heating anomaly in 2019/20 with the BCs from the three different years (Figures 8a–8c). The first column shows the impact of the Indian Ocean heating anomaly in different years with the (same) BCs of 2019/20 (Figure 8a, 8d and 8f). The diagonal panels (Figure 8a, 8e and 8g) show the impact of Indian Ocean heating in the reference experiments and are identical to Figures 6a–6c, which are reproduced here for ease of comparison. The figure shows that the stratospheric pathway is sensitive to both the BCs and to the characteristics of the Indian Ocean SST anomalies, in a non-linear manner. Specifically, Indian Ocean heating in 2019/20 produces a consistent strengthening of the SPV with the BCs of different years (first row of Figure 8). However, compared to 2019/20, the strengthening impact is of shorter duration with the BCs of

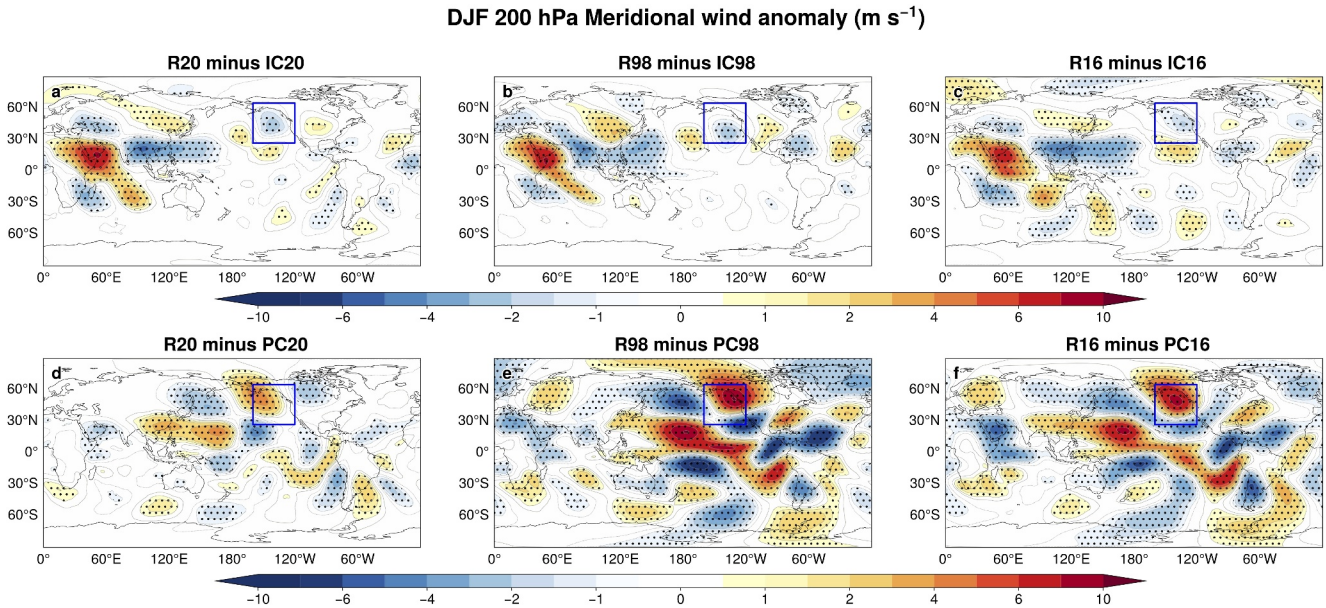

Figure 7. Same as Figure 5 but for 200 hPa meridional wind anomaly (m s^{-1}).

1997/98 (Figure 8b). In 2015/16, the impact is stronger in December but then weakens over time, such that by February, it is not as strong as in 2019/20.

The different Indian Ocean SST anomalies from the 3 years also produce a strengthening of the SPV with the BCs of 2019/20 (left column of Figure 8). The peak response (in January) is stronger with the 1997/98 Indian Ocean anomaly (Figure 8d) than with those of 2019/20 (Figure 8a) and 2015/16 (Figure 8f), but the strengthening does not reach the lower stratosphere (50–100 hPa) until later in the season. With the Indian Ocean SST anomaly from 2015/16, the strengthening of the westerlies reaches the lower stratosphere earlier (Figure 8f). Note that the 1997/98 anomaly produces a much weaker response in 1997/98 than with the BCs of 2019/20 (second row of Figure 8), indicating the strong sensitivity of the stratospheric pathway to the background state. On the other hand, the 2015/16 anomaly produces a much stronger response in 2015/16 than with the BCs of 2019/20 (bottom row in Figure 8). We conclude that the BCs of 1997/98 (2015/16) were the least (most) favorable for the stratospheric pathway. We also conclude that the intensity of the response of the SPV in 2015/16 (Figure 8g) cannot be adequately explained by a simple linear superposition of impacts of the background state and Indian Ocean anomaly.

Similar impact matrix for the tropospheric pathway is shown in Figure S4 in Supporting Information S1, in terms of the Rossby Wave Source at 200 hPa. The figure confirms that the tropospheric pathway appears more robust than the stratospheric pathway, although some differences appear on the North Atlantic when using either the 2015/16 Indian Ocean SST anomaly or the 2015/16 BCs, which could in turn be a manifestation of the stratospheric influence in the region.

The impact matrix for precipitation (Figure S5 in Supporting Information S1) shows that the structure of the Indian Ocean precipitation anomaly is mainly determined by the structure and amplitude of the local SST anomalies, with little sensitivity to the background conditions.

Figure 9 shows the distribution of the NAO index in the reference and attribution experiments. Like the impact on the SPV, the Indian Ocean heating anomaly from the 3 years, but with the same BCs of 2019/20, produces a similar and strong positive NAO response (Figures 9a, 9c, and 9d). However, when the Indian Ocean anomaly in 2019/20 is imposed on the BCs of 1997/98 and 2015/16, the impact on NAO is weaker than in R20 (Figures 9g and 9j compared to Figure 9a). This is consistent with the destructive interference between the strong Pacific El Niño conditions and the warm Indian Ocean, as we show in Figures 5–7. Both in 1997/98 and 2015/16 the impact of the Indian Ocean anomaly of 2019/20 would have been overshadowed by El Niño. These findings make the results of experiment R16 more remarkable, being the only experiment where the impact of the Indian Ocean SST outcompetes the effects of the strong Pacific forcing.

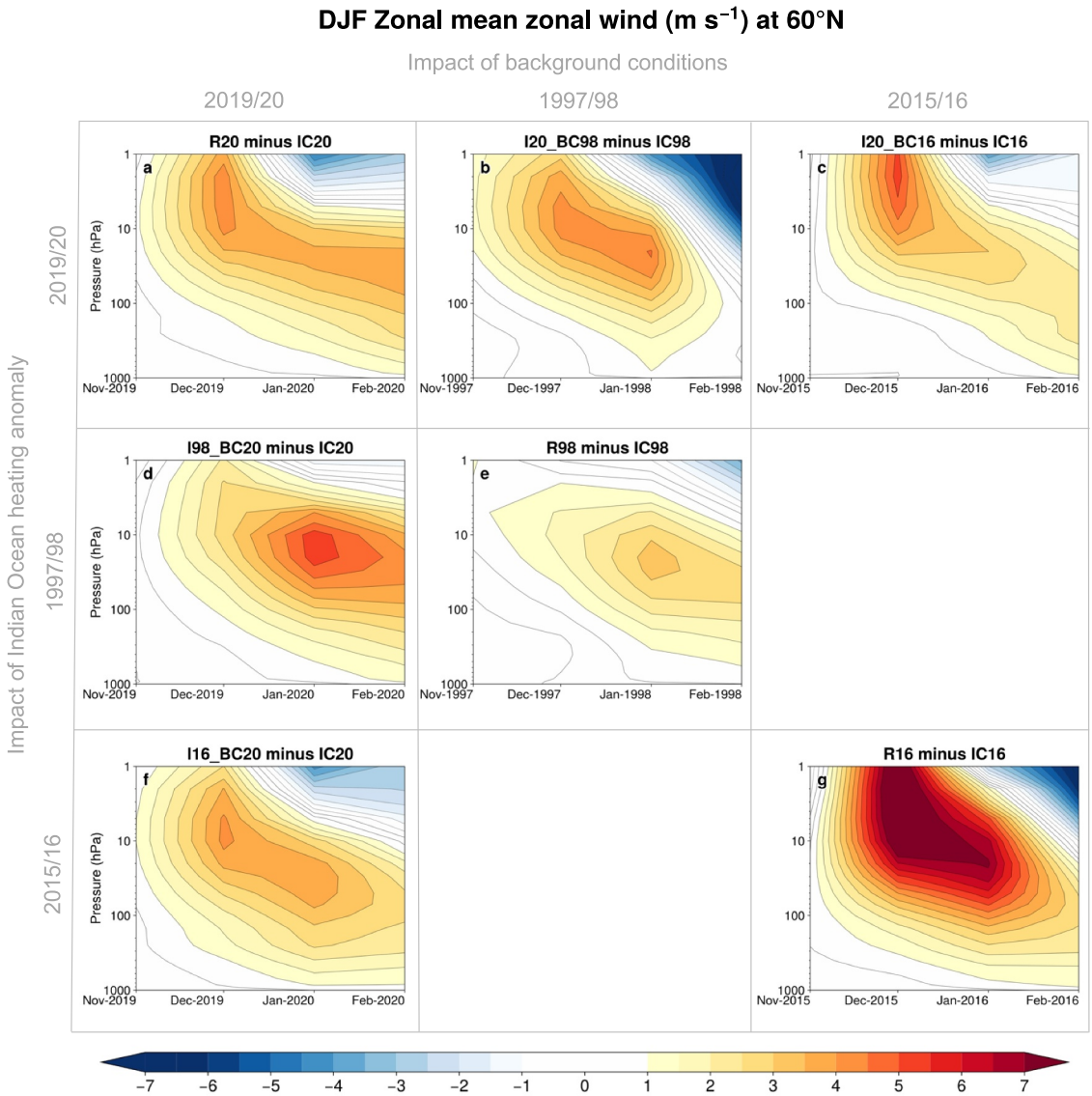

Figure 8. DJF seasonal mean zonal mean zonal wind (m s^{-1}) at 60°N plotted as ensemble mean differences between pairs of reference and attribution experiments contrasting the impact of the background conditions with the same Indian Ocean anomaly (first row), the impact of Indian Ocean heating anomaly in different years with the same background conditions of 2019/20 (first column) and the impact of Indian Ocean heating in the reference experiments (diagonal panels).

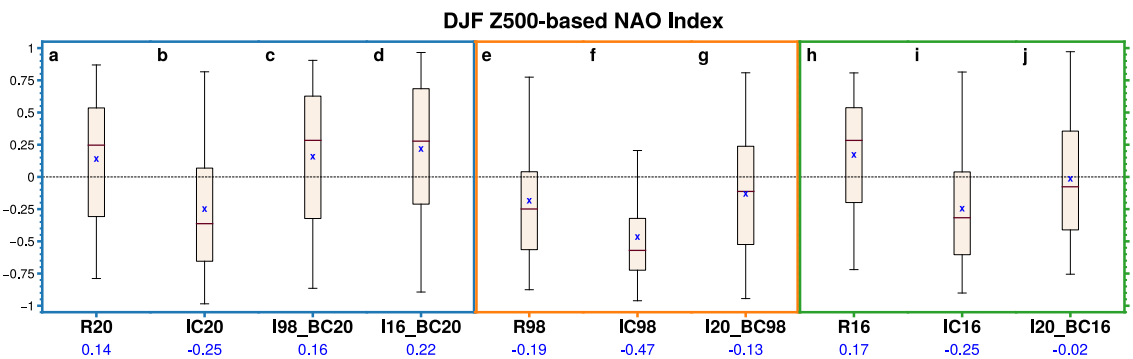

Figure 9. Box-and-whisker plots of the DJF mean NAO index for the reference and attribution experiments for 2019/20 (blue section), 1997/98 (orange section) and 2015/16 (green section). The ensemble mean values of the NAO index are overlaid as blue crosses as well as annotated in the *x*-axis.

3.3. Sources of Uncertainty in NAO Predictions

While the phase of the ensemble mean NAO in the reference experiments is correct, there is a large spread across the ensemble members (Figures 6g–6i). To gain insight into the reasons for this spread, we conduct two sets of intra-ensemble diagnostics: (a) we compare composites of the top (denoted by NAO+) and bottom (NAO−) 20 ensemble members sorted by their NAO indices and (b) we estimate the probabilities of the NAO conditioned on the SPV. These intra-ensemble diagnostics follow the spirit of Butler et al. (2014).

3.3.1. Intra-Ensemble Composites Conditioned on the NAO

By analyzing composites of NAO+ and NAO− within a given ensemble, we aim to identify features of the general atmospheric circulation associated with the occurrence of a given phase of the NAO, which can provide insight into sources of uncertainty.

The NAO± composites are constructed using the same subset of ensembles for each case study. Consequently, by construction, they share the same SST forcing, initial and boundary conditions. Therefore, any differences between composites highlight processes that contribute to uncertainty in the reforecasts. We are particularly interested in determining whether this uncertainty in NAO has a remote origin. If so, we would expect to observe it in the teleconnection pathways, Rossby wave sources or in the local response to SST anomalies.

The uncertainty in the NAO has a strong relation with the uncertainty in the SPV. The NAO+ composite consistently exhibits a strong SPV in the three reference experiments (Figures 10a–10c), while the NAO− composite shows a weak SPV (Figures 10d–10f). The vertical structure differs between the NAO+ and NAO− composites: in NAO+ members, westerly winds strengthen simultaneously in the troposphere and lower stratosphere, while in NAO− members, the signal propagates downwards from upper stratosphere, with similar characteristics to the downward propagation in the ensemble mean in Figure 6. The timing of the largest amplitude varies from year to year.

Members with strong positive NAO in 2019/20 also have a stronger tropospheric pathway (Figures 11a and 12a), with a clear Rossby wave train showing a negative node in 200 hPa winds over the Gulf of Alaska, with similar structure and amplitude as that in ERA5 (Figure 4a). We note that the negative Z500 anomaly region over the North Atlantic and Greenland in the R20 NAO+ composite (Figure 13a) is closer to observations (Figure 4a) than the ensemble mean anomaly, with the amplitude of the anomalies commensurable with those in ERA5. In contrast, the tropospheric pathway in the R20 NAO− composite (Figure 11d) is weaker already over the tropical Indian Ocean, and by the time it reaches the western side of the North American coast, has the opposite phase as the observations. The weaker wave train already at the source of the forcing is indicative of unpredictable processes in the Rossby wave response to the given SST anomaly (Figure 12). However, analysis of the Indian Ocean precipitation composites associated to NAO+ and NAO− show very similar amplitude and structure (Figure S6 in Supporting Information S1), and the spread among the NAO+ and NAO− ensemble members in precipitation anomalies over the western central Indian Ocean (Figure S6g–S6i in Supporting Information S1) is small and of the same sign. These results (larger uncertainty in Rossby wave source than in precipitation) are consistent with Strauss et al. (2023) who noted that the error growth in the Rossby wave source and its extratropical response is stronger than that of the heating itself.

During the El Niño years 1997/98 and 2015/16, the tropospheric pathway in both NAO+ and NAO− composites is similar over the Indo-Pacific region (Figures 11b, 11c, 11e and 11f), and in agreement with Figures 4e, 4f, 6e and 6f. The phase of the wave train in both composites is such that a positive wind anomaly is present off the North American west coast in both years, although the anomaly in the R16 NAO+ composite is weaker. The similarity of the tropospheric pathway for the El Niño years despite the difference in the NAO outcome suggests that the positive NAO seen in 2016 was largely due to variability associated with the SPV.

3.3.2. Probability of NAO Conditioned on the SPV Phases

In the previous section, we examined the uncertainty in atmospheric circulation conditioned on the phases of the NAO. Here, we assess the probabilities for the occurrence of NAO conditioned on a given state of the atmospheric circulation, again using intra-ensemble diagnostics for different cases. We focus on how the SPV conditions the probability of NAO in the different ensembles. By comparing how these probabilities change between the different experiments, these diagnostics also shed light on how the tropical SST affects the SPV.

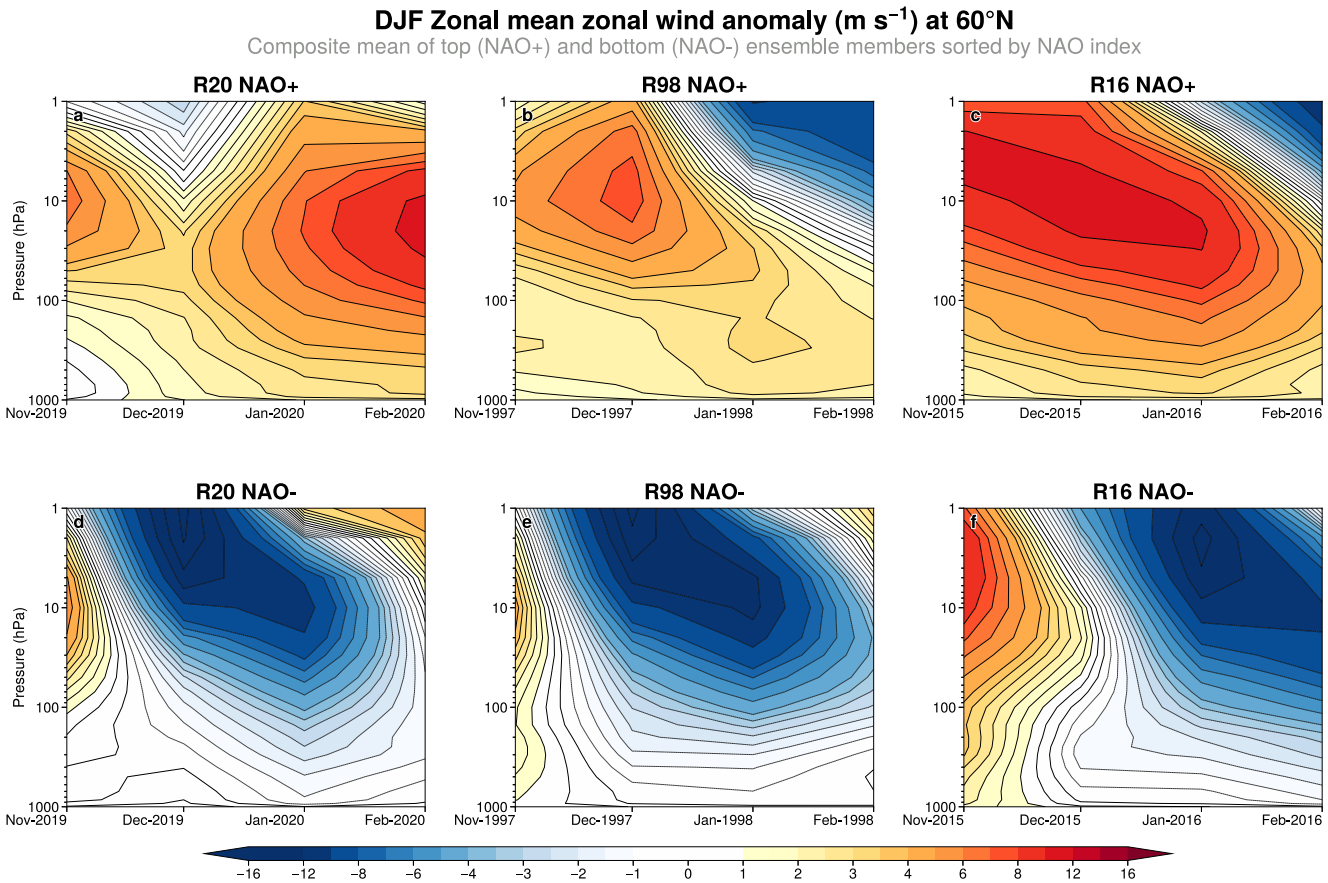

Figure 10. DJF seasonal mean zonal mean zonal wind anomaly (m s^{-1}) at 60°N from (a) and (d) R20, (b) and (e) R98, (c) and (f) R16 plotted as a composite of the top (NAO+, upper panel) and bottom (NAO−, lower panel) 20 ensemble members sorted by their NAO indices.

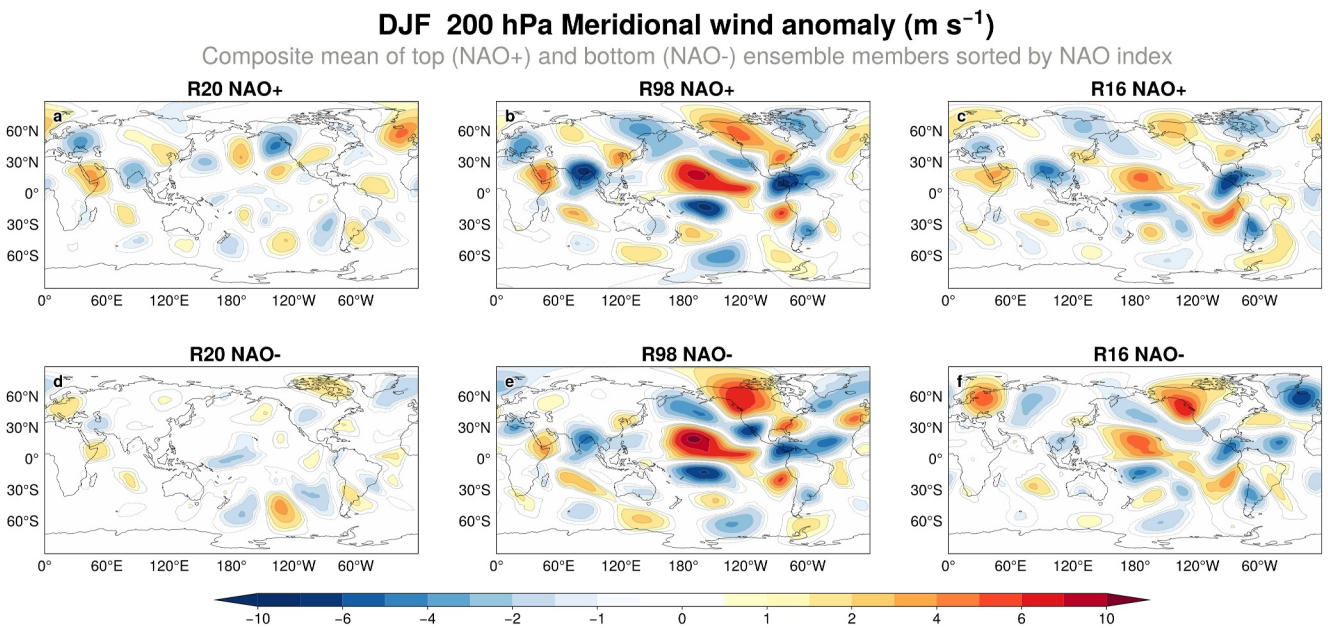

Figure 11. DJF seasonal mean 200 hPa Meridional wind anomaly (m s^{-1}) from (a) and (d) R20, (b) and (e) R98, (c) and (f) R16 plotted as composites of the top (NAO+, upper panel) and bottom (NAO−, lower panel) 20 ensemble members sorted by their NAO indices.

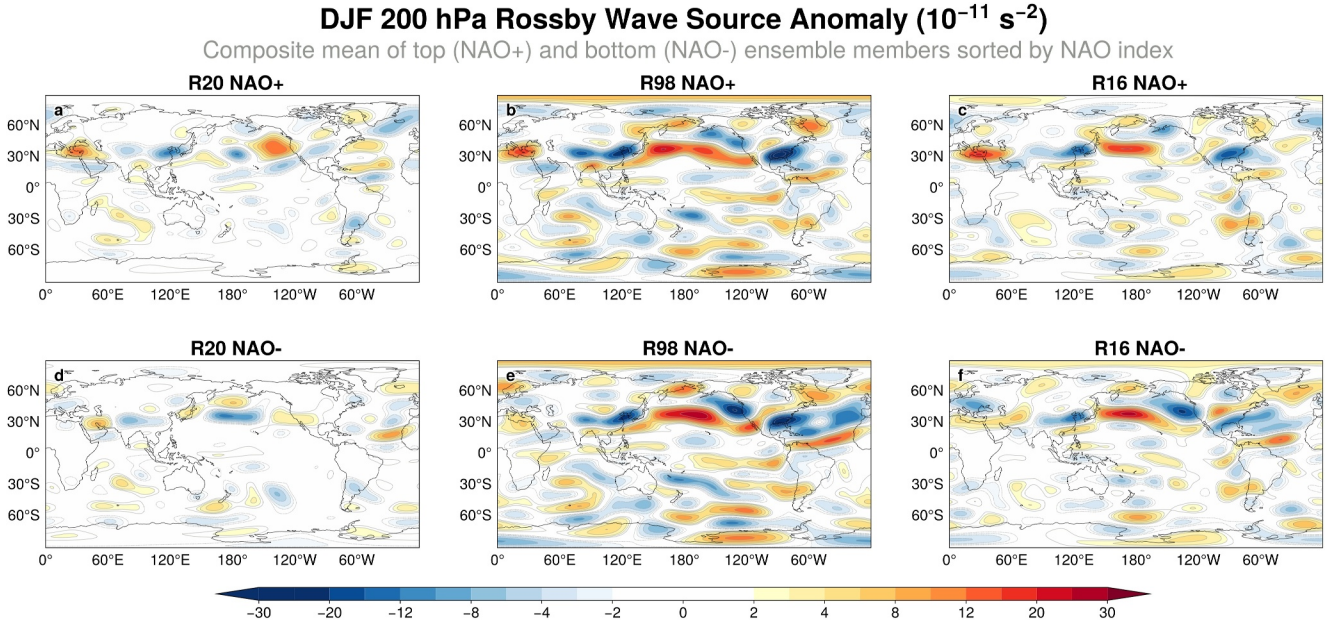

Figure 12. Same as Figure 11, but for Rossby wave source anomaly (10^{-11} s^{-2}).

Figure 14 shows scatter diagrams of the SPV index (denoted by the 100 hPa DJF mean zonal mean zonal wind anomaly at 60ºN) against the NAO index for the R and IC experiments (for the interested reader, see Figure S7 in Supporting Information S1 for scatter diagrams with the SPV index defined at other levels). Figure 15a condenses the information by displaying the relationship between the probability of the SPV+ (P^{SPV+}) and the probability of NAO+ conditioned on the occurrence of the SPV+ (P^{NAO+}_{SPV+}), for different levels of the SPV. Figure 15b is the equivalent diagram for P^{SPV-} and P^{NAO-}_{SPV-}. Companion diagrams in Figures 15c and 15d compare the probability of NAO+/NAO− (P^{NAO+}/P^{NAO-}) related with the SPV+ ($P^{NAO+}_{SPV+} \times P^{SPV+}$)/SPV-($P^{NAO-}_{SPV-} \times P^{SPV-}$), where the distance of the points to the diagonal is indicative of other factors leading to NAO unrelated to the SPV. The probabilities are estimated by the fraction of ensemble members in each quadrant of Figure 14 with respect to the

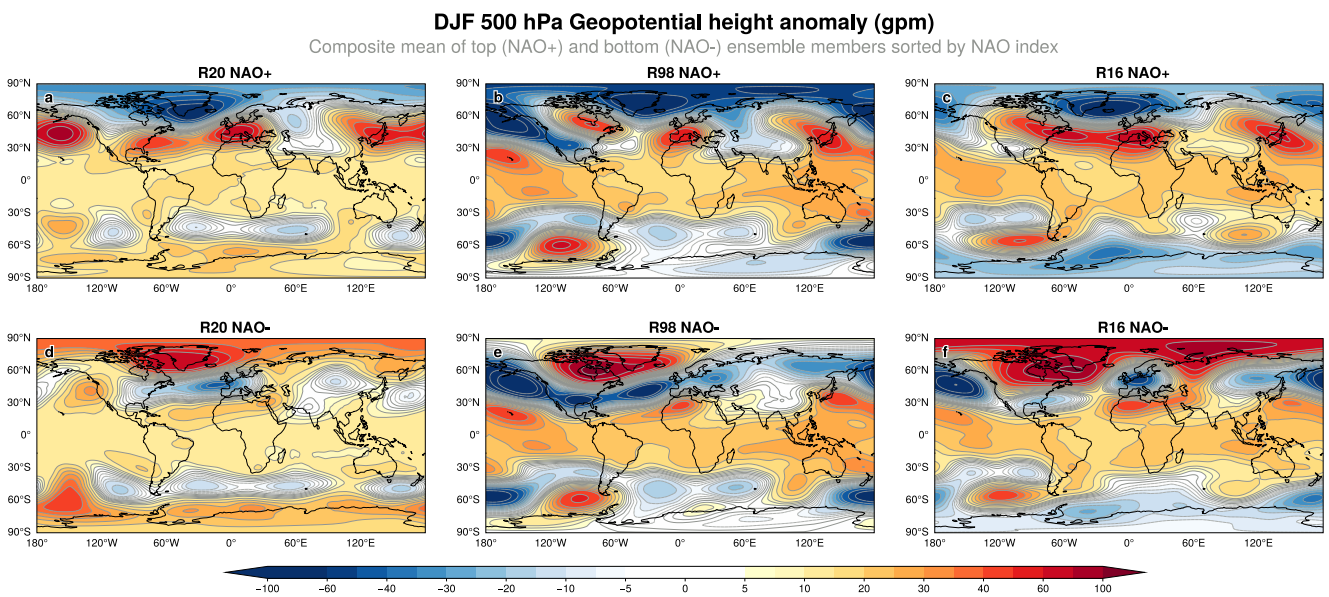

Figure 13. DJF seasonal mean 500 hPa Geopotential height anomaly (gpm) from R20 (left panel), R98 (middle panel) and R16 (right panel) plotted as composites of the top (NAO+) and bottom (NAO−) 20 ensemble members sorted by their NAO indices.

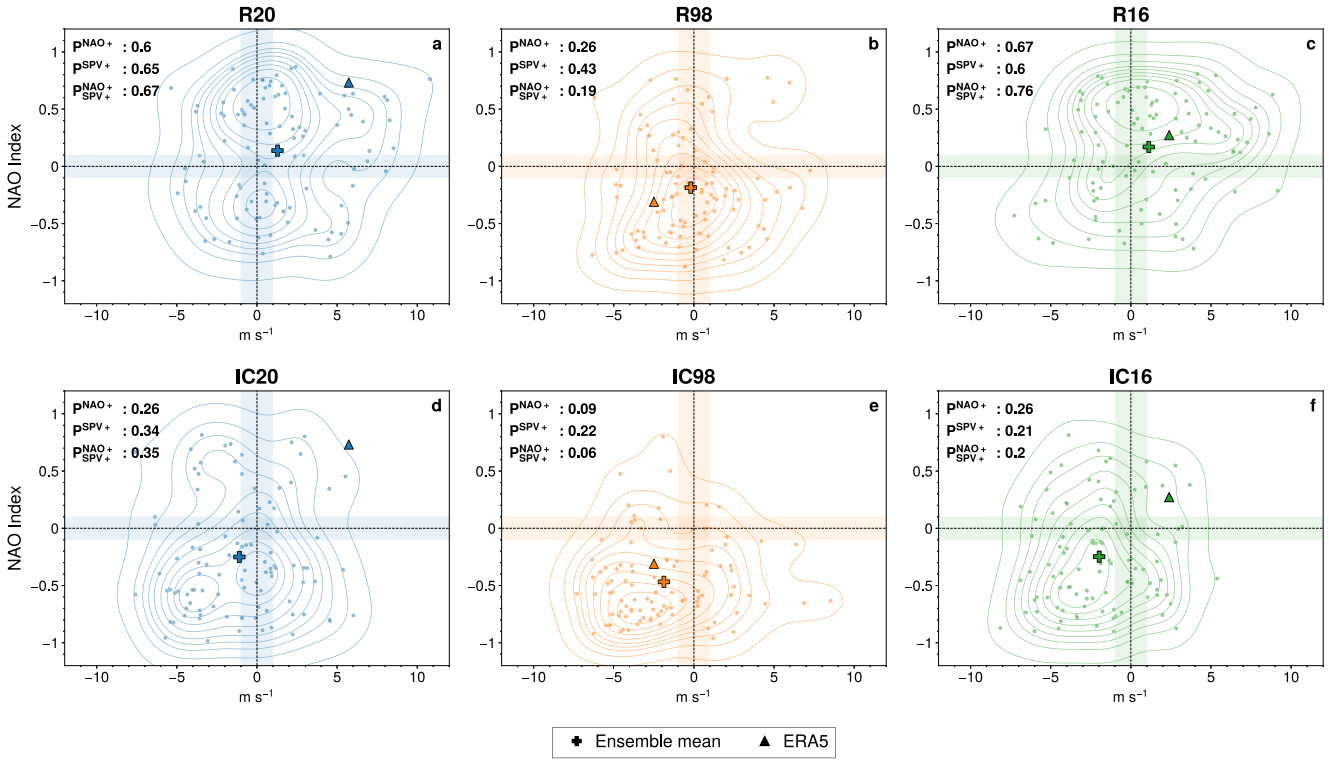

Figure 14. DJF mean 100 hPa zonal mean zonal wind anomaly at 60°N (m s^{-1}) plotted as scatter diagram against the DJF mean NAO Index for the R (top panels) and IC (bottom panels) experiments. The associated kernel density estimation contours are overlaid. Also plotted are the ensemble mean (plus symbol) and ERA5 (triangle symbol). The probability estimates for the occurrence of positive phase of NAO (P^{NAO+}), strong SPV (P^{SPV+}) and of positive NAO conditioned on strong SPV (P^{NAO+}_{SPV+}) are listed.

total number (the top/bottom quadrants for P^{NAO+}/P^{NAO-}, right/left quadrants for P^{SPV+}/P^{SPV-}, upper-right quadrant for P^{NAO+}_{SPV+} and lower-left quadrant for P^{NAO-}_{SPV-}). The ensemble members falling in the shaded zone around zero have been excluded.

Removing the Indian Ocean SST anomalies clearly decreases the probability of NAO+, SPV+ and P^{NAO+}_{SPV+} - especially noticeable in R20/IC20 and R16/IC16 (Figures 14, 15a and 15c) - while increasing the probability of NAO−, SPV− and P^{NAO-}_{SPV-} across the 3 years (Figures 14, 15b and 15d). These results confirm the idea that interferences between the Indian and Pacific Ocean contributed to source of uncertainty in NAO. In all 3 years, the IC experiments increase the probability of SPV− and NAO− (Figures 14d–14f) as anticipated by the results presented in previous sections.

Among the reference experiments, R16 has the second highest P^{SPV+} and the highest P^{NAO+}_{SPV+} even in the presence of El Niño (Figure 15a). These probabilities are consistently high in the vertical, with relatively high values also at 10 hPa (note the smallest horizontal separation between green filled circles in Figure 15a). This can be further confirmed in Figures S7j, S7k and S7l in Supporting Information S1. Compared to other years, the Indian Ocean SST in 2015/16 had the largest impact on SPV+ and its NAO+ conditioning across all levels (Figure 15a). In IC16, the probability of NAO− is almost entirely associated with SPV− (green filled squares closest to the diagonal in Figure 15d).

SPV+ in R20 is similar to R16, but P^{SPV+} exhibit a faster decrease with height (larger horizontal spacing in Figure 15a). Besides P^{NAO+}_{SPV+} is weaker in R20 than in R16. This behavior suggests that the ability of the SPV+ to influence the NAO+ may depend on the coherence of the vertical structure of the SPV. Removing the Indian Ocean SST anomalies in IC20 decreases the probability of P^{SPV+} and P^{NAO+}_{SPV+}, but its impact is not as noticeable as in IC16.

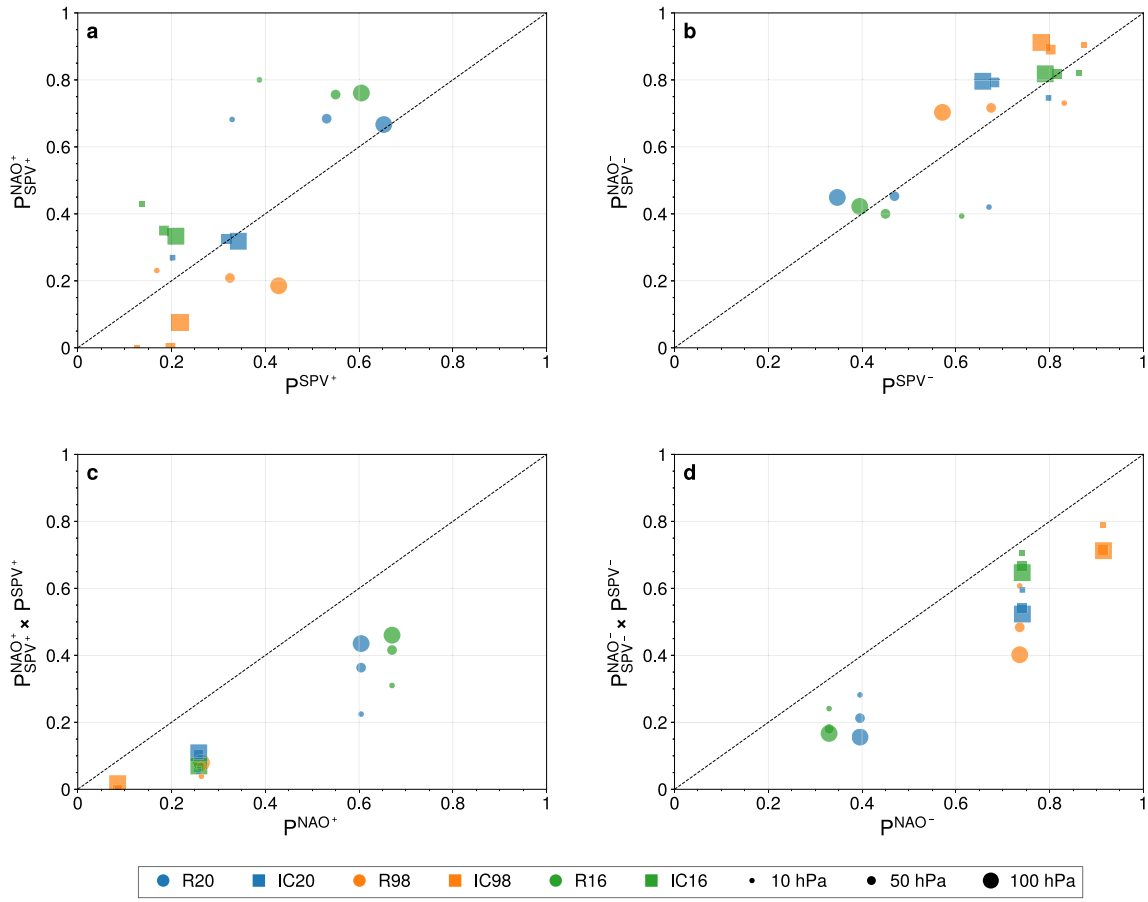

Figure 15. Scatter diagram of probabilities (a) P^{SPV+} against P^{NAO+}_{SPV+} (b) P^{SPV-} against P^{NAO-}_{SPV-} (c) $P^{NAO+}_{SPV+} \times P^{SPV+}$ against P^{NAO+} and (d) $P^{NAO-}_{SPV-} \times P^{SPV-}$ against P^{NAO-}, for the R (filled circle) and IC (filled square) experiments for 10 hPa (small-size circle/square), 50 hPa (medium-size circle/square and 100 hPa (large-size circle/square).

R98 shows the lowest probability of SPV+ and weak conditioning on NAO+ by the SPV (Figures 14b, 15a and 15c), consistent with the El Niño in the Pacific favoring a weak SPV. These probabilities decrease further in the corresponding IC98 experiment (Figures 14e, 15a and 15c). Compared to the other years, SPV− contributes to increase the probability of NAO− in R98 (orange filled circles in Figures 15b and 15d), and this contribution is substantially increased in IC98 (orange filled squares in Figures 15b and 15d), supporting the idea that the stratospheric pathway is behind the competing influence of the Indian and Pacific Ocean on the NAO. They also support the existence of a constructive interference between tropospheric and stratospheric pathways associated with ENSO forcing.

In summary, there is a clear year-to-year variation in the probabilities of the phases of SPV and its association with the NAO. The Indian Ocean state plays an important role for these variations, although it is not always the dominant factor. It is the strongest factor in R16 and the weakest in R98.

The results in Figures 14 and 15 support three of the main outcomes of this study, namely: (a) the role of the stratospheric pathway as mediator of teleconnections from individual ocean basins, (b) the exceptional nature of the stratospheric pathway in 2015/16; and (c) the interference between the tropical forcing in different basins.

The analysis conducted in this section focuses not only on the relationship between stratospheric pathway and the NAO, but it also provides some information on factors other than the SPV related with NAO (i.e., distance to diagonal in Figures 15c and 15d), which likely comprise the tropospheric pathway. To complete the overall picture, it would be desirable to conduct a similar analysis of probabilities for the tropospheric pathway. However, given the complexities involved in defining and interpreting an objective index for the tropospheric pathway, this task is beyond the scope of the current study and is best addressed in future research.

4. Summary and Conclusions

Results from large ensemble atmospheric seasonal reforecast experiments with combinations of prescribed SST anomalies for three different winters show a response of NAO to tropical heating from the western-central Indian Ocean. The teleconnection is established via both a tropospheric and a stratospheric pathway. The tropospheric pathway is robust across the three winters and has the footprint of a quasi-stationary Rossby wave train that manifests locally as a dipole in 200 hPa meridional wind (positive pole over the Arabian Peninsula, negative pole over Indian subcontinent), and remotely with negative anomalies over Gulf of Alaska. The stratospheric pathway is associated with a consistent strengthening of the SPV, that nevertheless displays large variability within a given ensemble.

In agreement with previous studies (FC15; Fletcher & Kushner, 2011; Molteni et al., 2015), results from three winter seasons show that the NAO response to El Niño is in opposite phase with that due to the Indian Ocean. In our results, the competing influence of the two basins is visible in both the tropospheric and stratospheric pathways. This interference from forcing between the two basins is different in the three cases considered and along with the SPV variability leads to the spread in the NAO. Note that this destructive interference between basins is different from that pointed out by FC15, which refers to a linear interference between anomalous and climatological Rossby waves, not considered here.

In 2019/20, the Indian Ocean SST was largely the sole tropical driver for the positive NAO, with only a weak destructive interference from the tropical Pacific basin (2019/20 was ENSO neutral). Despite this lack of interference, the seasonal predictions of NAO exhibited large spread. Part of that spread could be attributable to the Rossby wave response to the tropical heating, and an additional part to intrinsic variability of the SPV.

In 1997/98 there was a negative NAO resulting from the large El Niño that winter, even though the Indian Ocean forcing was strong. Results suggest that had there not been El Niño in 1997/98, the Indian Ocean would have produced a positive NAO signal, as occurred in 2019/20 and 2015/16. In the latter, the interference between the Pacific and Indian Ocean was a major contributor to the uncertainty in the NAO predictions, with visible impact on the spread.

In 2015/16, the balance between Indian and Pacific forcings tilted in favor of the Indian Ocean, resulting in a positive NAO despite the strong El Niño forcing. This case shows the strongest stratospheric response to the Indian Ocean heating, but the reasons for the sensitivity in this particular year are still to be understood.

Intra-ensemble composites indicate that uncertainty in the NAO forecasts is associated with unconstrained variability in the atmospheric response to a local SST anomaly and with the internal variability of the SPV.

The above results highlight the flow-dependent nature of the predictability at seasonal time scales. Although this is not strictly a new result, it is an important aspect to bear in mind when explaining a given seasonal forecast. It is also important for interpreting the information provided by standard skill metrics, which does not include the concept of windows of opportunity.

The findings presented in this paper have implications for understanding how climate change affects mid latitude atmospheric circulation. The Indian Ocean is the basin where SSTs have warmed most rapidly due to climate change (e.g., Guemas et al., 2013; Wenegrat et al., 2022). If increased SST anomalies lead to increased tropical heating, triggering atmospheric teleconnections, the results of this study suggest that this will favor the occurrence of a positive NAO. However, the efficiency of tropical SST in triggering deep convection and teleconnections remains to be understood, quantified and modeled (e.g., Copsey et al., 2006).

Finally, we remark that this study is based on atmosphere-only simulations, which on one hand cannot account for coupled feedback between the atmosphere and the underlying ocean which can affect the solution, such as air-sea interaction affecting diabatic heating, both in the tropics or locally in the North Atlantic, but on the other are not affected by SST biases present in the coupled model. We also note that the information discussed in this study necessitated a large ensemble size, consistent with Eade et al. (2014), larger than the one provided by current operational seasonal forecasting systems.

Data Availability Statement

ERA5 daily sea surface temperature and total precipitation, as well as monthly mean pressure level data for geopotential, zonal and meridional wind, are publicly available from the ECMWF C3S Climate Data Store (CDS) (Hersbach et al., 2023a, 2023b). The data from the atmosphere-only seasonal reforecast experiments used in this study (ECMWF, 2023a; ECMWF, 2023b; ECMWF, 2023c; ECMWF, 2023d; ECMWF, 2023e; ECMWF, 2023f; ECMWF, 2023g; ECMWF, 2023h; ECMWF, 2023i; ECMWF, 2024a; ECMWF, 2024b; ECMWF, 2024c; ECMWF, 2024d) are available under a Creative Commons Attribution 4.0 International license (CC BY 4.0). To view a copy of this license, visit https://creativecommons.org/licenses/by/4.0/.

Acknowledgments
This research was partially supported by the European Union's research and innovation programmes: Horizon 2020 (Grant agreement no. 101004156, CONFESS project) and Horizon Europe (Grant agreement no. 101081460, ASPECT Project).

References

Abid, M. A., Kucharski, F., Molteni, F., Kang, I.-S., Tompkins, A. M., & Almazroui, M. (2021). Separating the Indian and Pacific Ocean impacts on the Euro-Atlantic response to ENSO and its transition from early to late winter. *Journal of Climate*, *34*(4), 1531–1548. https://doi.org/10.1175/JCLI-D-20-0075.1

Bader, J., & Latif, M. (2005). North Atlantic oscillation response to anomalous Indian Ocean SST in a coupled GCM. *Journal of Climate*, *18*(24), 5382–5389. https://doi.org/10.1175/JCLI3577.1

Brönnimann, S. (2007). Impact of El Niño–Southern oscillation on European climate. *Reviews of Geophysics*, *45*(3). https://doi.org/10.1029/2006RG000199

Butler, A. H., Polvani, L. M., & Deser, C. (2014). Separating the stratospheric and tropospheric pathways of El Niño–Southern oscillation teleconnections. *Environmental Research Letters*, *9*(2), 024014. https://doi.org/10.1088/1748-9326/9/2/024014

Copsey, D., Sutton, R., & Knight, J. R. (2006). Recent trends in sea level pressure in the Indian Ocean region. *Geophysical Research Letters*, *33*(19). https://doi.org/10.1029/2006GL027175

Domeisen, D. I. V., Butler, A. H., Charlton-Perez, A. J., Ayarzagüena, B., Baldwin, M. P., Dunn-Sigouin, E., et al. (2020). The role of the stratosphere in subseasonal to seasonal prediction: 2. Predictability arising from stratosphere-troposphere coupling. *Journal of Geophysical Research: Atmospheres*, *125*(2), e2019JD030923. https://doi.org/10.1029/2019JD030923

Domeisen, D. I. V., Garfinkel, C. I., & Butler, A. H. (2019). The teleconnection of El Niño southern oscillation to the stratosphere. *Reviews of Geophysics*, *57*(1), 5–47. https://doi.org/10.1029/2018RG000596

Dunstone, N., Smith, D., Scaife, A., Hermanson, L., Eade, R., Robinson, N., et al. (2016). Skilful predictions of the winter North Atlantic Oscillation one year ahead. *Nature Geoscience*, *9*(11), 809–814. https://doi.org/10.1038/ngeo2824

Eade, R., Smith, D., Scaife, A., Wallace, E., Dunstone, N., Hermanson, L., & Robinson, N. (2014). Do seasonal-to-decadal climate predictions underestimate the predictability of the real world? *Geophysical Research Letters*, *41*(15), 5620–5628. https://doi.org/10.1002/2014GL061146

ECMWF. (2023a). Indian Ocean SST attribution experiment for winter 1997/98: IC98. *ECMWF*. https://doi.org/10.21957/DMER-9573

ECMWF. (2023b). Indian Ocean SST attribution experiment for winter 2015/16: IC16. *ECMWF*. https://doi.org/10.21957/B7PR-2Z60

ECMWF. (2023c). Indian Ocean SST attribution experiment for winter 2019/20: IC20. *ECMWF*. https://doi.org/10.21957/0WDB-3Q97

ECMWF. (2023d). Pacific Ocean SST attribution experiment for winter 1997/98: PC98. *ECMWF*. https://doi.org/10.21957/QRSY-E285

ECMWF. (2023e). Pacific Ocean SST attribution experiment for winter 2015/16: PC16. *ECMWF*. https://doi.org/10.21957/EJ5P-FK14

ECMWF. (2023f). Pacific Ocean SST attribution experiment for winter 2019/20: PC20. *ECMWF*. https://doi.org/10.21957/YTKB-FB06

ECMWF. (2023g). Reference seasonal experiment for winter 1997/98: R98. *ECMWF*. https://doi.org/10.21957/NDKM-NR53

ECMWF. (2023h). Reference seasonal experiment for winter 2015/16: R16. *ECMWF*. https://doi.org/10.21957/KGTN-V960

ECMWF. (2023i). Reference seasonal experiment for winter 2019/20: R20. *ECMWF*. https://doi.org/10.21957/EJAN-GB83

ECMWF. (2024a). Attribution experiment for winter 1997/98 with Indian Ocean SST anomaly of 2019/20: I20_BC98. *ECMWF*. https://doi.org/10.21957/xd6h-rr82

ECMWF. (2024b). Attribution experiment for winter 2015/16 with Indian Ocean SST anomaly of 2019/20: I20_BC16. *ECMWF*. https://doi.org/10.21957/9x89-4c27

ECMWF. (2024c). Attribution experiment for winter 2019/20 with Indian Ocean SST anomaly of 1997/98: I98_BC20. *ECMWF*. https://doi.org/10.21957/203z-v321

ECMWF. (2024d). Attribution experiment for winter 2019/20 with Indian Ocean SST anomaly of 2015/16: I16_BC20. *ECMWF*. https://doi.org/10.21957/3n48-t818

Fletcher, C. G., & Cassou, C. (2015). The dynamical influence of separate teleconnections from the Pacific and Indian Oceans on the northern annular mode. *Journal of Climate*, *28*(20), 7985–8002. https://doi.org/10.1175/JCLI-D-14-00839.1

Fletcher, C. G., & Kushner, P. J. (2011). The role of linear interference in the annular mode response to tropical SST forcing. *Journal of Climate*, *24*(3), 778–794. https://doi.org/10.1175/2010JCLI3735.1

Garfinkel, C. I., Benedict, J. J., & Maloney, E. D. (2014). Impact of the MJO on the boreal winter extratropical circulation. *Geophysical Research Letters*, *41*(16), 6055–6062. https://doi.org/10.1002/2014GL061094

Guemas, V., Corti, S., García-Serrano, J., Doblas-Reyes, F. J., Balmaseda, M., & Magnusson, L. (2013). The Indian ocean: The region of highest skill worldwide in decadal climate prediction. *Journal of Climate*, *26*(3), 726–739. https://doi.org/10.1175/JCLI-D-12-00049.1

Hardiman, S. C., Dunstone, N. J., Scaife, A. A., Smith, D. M., Knight, J. R., Davies, P., et al. (2020). Predictability of European winter 2019/20: Indian Ocean Dipole impacts on the NAO. *Atmospheric Science Letters*, *21*(12). https://doi.org/10.1002/asl.1005

Hersbach, H., Bell, B., Berrisford, P., Biavati, G., Horányi, A., Muñoz Sabater, J., et al. (2023a). ERA5 hourly data on single levels from 1940 to present. *Copernicus Climate Change Service (C3S) Climate Data Store (CDS)*. https://doi.org/10.24381/cds.adbb2d47

Hersbach, H., Bell, B., Berrisford, P., Biavati, G., Horányi, A., Muñoz Sabater, J., et al. (2023b). ERA5 monthly averaged data on pressure levels from 1940 to present. *Copernicus Climate Change Service (C3S) Climate Data Store (CDS)*. https://doi.org/10.24381/cds.6860a573

Hersbach, H., Bell, B., Berrisford, P., Hirahara, S., Horányi, A., Muñoz-Sabater, J., et al. (2020). The ERA5 global reanalysis. *Quarterly Journal of the Royal Meteorological Society*, *146*(730), 1999–2049. https://doi.org/10.1002/qj.3803

Hurrell, J. W., Kushnir, Y., Ottersen, G., & Visbeck, M. (2003). An overview of the North Atlantic oscillation. In *The North Atlantic oscillation: Climatic significance and environmental impact* (pp. 1–35). American Geophysical Union (AGU). https://doi.org/10.1029/134GM01

Johnson, S. J., Stockdale, T. N., Ferranti, L., Balmaseda, M. A., Molteni, F., Magnusson, L., et al. (2019). SEAS5: The new ECMWF seasonal forecast system. *Geoscientific Model Development*, *12*(3), 1087–1117. https://doi.org/10.5194/gmd-12-1087-2019

Lee, S. H., Lawrence, Z. D., Butler, A. H., & Karpechko, A. Y. (2020). Seasonal forecasts of the exceptional northern hemisphere winter of 2020. *Geophysical Research Letters*, *47*(21). https://doi.org/10.1029/2020GL090328

Li, J., & Wang, J. X. L. (2003). A new North Atlantic Oscillation index and its variability. *Advances in Atmospheric Sciences*, *20*(5), 661–676. https://doi.org/10.1007/BF02915394

Molteni, F., Stockdale, T. N., & Vitart, F. (2015). Understanding and modelling extra-tropical teleconnections with the Indo-Pacific region during the northern winter. *Climate Dynamics*, *45*(11), 3119–3140. https://doi.org/10.1007/s00382-015-2528-y

Roberts, C. D., Balmaseda, M. A., Ferranti, L., & Vitart, F. (2023). Euro-Atlantic weather regimes and their modulation by tropospheric and stratospheric teleconnection pathways in ECMWF reforecasts. *Monthly Weather Review*, *151*(10), 2779–2799. https://doi.org/10.1175/MWR-D-22-0346.1

Stockdale, T. (2021). SEAS5 user guide Version 1.2. *ECMWF*. https://doi.org/10.21957/2y67999y

Straus, D. M., Domeisen, D. I. V., Lock, S.-J., Molteni, F., & Yadav, P. (2023). Intrinsic predictability limits arising from Indian ocean Madden–Julian oscillation (MJO) heating: Effects on tropical and extratropical teleconnections. *Weather Clim. Dynam.*, *4*, 1001–1018. https://doi.org/10.5194/wcd-4-1001-2023

Toniazzo, T., & Scaife, A. A. (2006). The influence of ENSO on winter North Atlantic climate. *Geophysical Research Letters*, *33*(24). https://doi.org/10.1029/2006GL027881

Trenberth, K. E., Branstator, G. W., Karoly, D., Kumar, A., Lau, N.-C., & Ropelewski, C. (1998). Progress during TOGA in understanding and modeling global teleconnections associated with tropical sea surface temperatures. *Journal of Geophysical Research*, *103*(C7), 14291–14324. https://doi.org/10.1029/97JC01444

Vitart, F., Emerton, R., Rodwell, M., Alonso-Balmaseda, M., Haiden, T., Johnson, S., et al. (2022). Investigating biases in the representation of the Pacific sub-tropical jet stream and associated teleconnections (a UGROW sub-project). *ECMWF Technical Memoranda. ECMWF*. https://doi.org/10.21957/jcfqpdr2

Wang, G., Cai, W., Yang, K., Santoso, A., & Yamagata, T. (2020). A unique feature of the 2019 extreme positive Indian Ocean Dipole event. *Geophysical Research Letters*, *47*(18), e2020GL088615. https://doi.org/10.1029/2020GL088615

Wenegrat, J. O., Bonanno, E., Rack, U., & Gebbie, G. (2022). A century of observed temperature change in the Indian ocean. *Geophysical Research Letters*, *49*(13), e2022GL098217. https://doi.org/10.1029/2022GL098217